ОБЪЕДИНЕННЫЙ
ИНСТИТУТ
ЯДЕРНЫХ
ИССЛЕДОВАНИЙ
ДУБНА



D2 - 9789

M.S.Dubovikov, B.Z.Kopeliovich, L.I.Lapidus,
K.A.Ter-Martirosyan

# DYNAMICS OF FROISSARONS IN HIGH ENERGY PHYSICS

1976

D2 - 9789

M.S.Dubovikov,[1] B.Z.Kopeliovich, L.I.Lapidus,
K.A.Ter-Martirosyan[2]

# DYNAMICS OF FROISSARONS IN HIGH ENERGY PHYSICS

*Submitted to "Nuclear Physics"*

[1] Moscow Physical-Technical Institute, Moscow, USSR.

[2] Institute of Theoretical and Experimental Physics, Moscow, USSR.

Дубовиков М.С. и др. **D2 - 9789**

Динамика фруассаронов в физике высоких энергий

Теория померона с $\alpha(0) > 1$ позволяет получить при высоких энергиях хорошее описание экспериментальных данных о бинарных реакциях и процессах множественного рождения частиц. При сверхвысоких энергиях $(\alpha(0)-1)\ln s \gg 1$ форма теории полностью меняется. В рассеянии адронов доминирует вклад нового объекта - "фруассарона", представляющего собой поток померонов, эффективное число которых растет как $(s/s_0)^{\alpha(0)-1}/\ln^2(s/s_0)$. Полные сечения в асимптотике растут по фруассаровскому закону, а средняя множественность как $(s/s_0)^{\alpha(0)-1}/\ln(s/s_0)$. Просуммирована совокупность всех померонных графиков и получено уравнение для точной функции Грина. Решением этого уравнения может быть Фруассарон. Вклад усиленных графиков эффективно уменьшает величину $\alpha(0)$ . Благодаря этому происходит смена асимптотического режима.

Работа выполнена в Лаборатории ядерных проблем, ОИЯИ.

Препринт Объединенного института ядерных исследований

Дубна 1976

Dubovikov M.S. et al. **D2 - 9789**

Dynamics of Froissarons in High Energy Physics

The Pomeron theory with $\alpha(0)=1+\Delta>1$ is considered. Some consequences of hadron scattering at accessible and asymptotic energies are formulated. At modern energies the small Pomeron intercept shift leads only to subtle effects. But in the region of $\ln(s/m^2)\cdot\Delta \gg 1$ the theory changes drastically. Hadron reactions are governed by a new object, "a Froissaron", which is a result of the multi-Pomeron exchange. The method for summing up the enhanced Froissaron graphs has been proposed which leads to an equation for the exact Green function. It is shown that under some restrictions on the Froissaron coupling the Froissaron can satisfy this equation, and the effect of enhanced graphs is reduced mainly to the renormalization of the $\Delta$-value. Thus, the problem of the s-channel unitarity has been also solved.

**Preprint of the Joint Institute for Nuclear Research**

**Dubna 1976**

## 1. Introduction

The increase of total hadron-hadron cross sections at high energies has been firstly predicted[1,2]) in the Pomeron theory with $\alpha_P(0) = 1$. It has been obtained there due to the decrease of the negative Regge cut contribution related to the exchange by two or more Pomerons. In this approach the growth rate of $\sigma_{tot.}(s)$ can be obtained, in the eikonal or quasi-eikonal approximation, from the experimental data on the diffraction cone slope B(s) and on the diffraction particle production cross section. The corresponding estimates[3]) have predicted the value of the order of 2-3% for the ratio $(d\sigma_{tot.}/d\ln s)/\sigma_{tot.}$. A considerably larger value, of the order of 6-7%, was obtained later[4,5]) experimentally. It was found impossible to eliminate this discrepancy by only changing the shape of the t-dependence of Regge vertices. Moreover, the inclusion of enhanced graphs[6]) makes the situation even worse. It has occurred, ref.[7]), that an enhanced graph correction to the Regge vertices dominates, leading to the decrease of $(d\sigma_{tot.}/d\ln s)/\sigma_{tot.}$ over the whole region of available energies.

In order to solve this problem the intercept of the Pomeron has been taken larger than unity[8,9]). In such a theory the Pomeron contribution due to its power rise $s^{\alpha(0)-1}$ violates itself the s-channel unitarity. But taking into account rescattering processes restores at least the two-particle s-unitarity. Cheng and Wu[10]) have been the first to show this in the model with a fixed Regge pole at $j = \alpha(t) = 1 + \Delta = \text{const}$. They have obtained good description for experimental data on the total and elastic differential cross sections. However, the problems of particle production and the proof of the many-particle s-unitarity remained quite subtle for this model.

In the theory with a moving pole a Feynmann ladder diagram may correspond to every Pomeron. The representation of the Pomeron as a ladder type graph contribution allows one to obtain the connection between elastic and different inelastic processes. For example, Abramovsky, Gribov, and Kanchely[11]) have obtained connection between the contribution of Regge cuts to the elastic scattering amplitude and inelastic processes with large multiplicity. At accessible energies the small shift of the Pomeron intercept $\alpha(0) = 1 + \Delta$ does not change radically the theoretical scheme. At the same time, the corresponding correction arising in the amplitude allow the description of experimental data on cross sections. The contribution of the Pomeron to the scattering amplitude behaves at accelerator energies as $(s/m^2)^{\Delta}$. However, at ultrahigh energies, when $(\ln s/m^2)\Delta \gg 1$ this behaviour drastically changes. The value of rescattering terms increases so much that the contribution of each term violates the s-channel unitarity. Nevertheless, their sum does not violate the unitarity condition because of cancellations of terms with different signs. So, the whole sum of all terms saturates the Froissart limit and asymptotically $\sigma_{tot.} \propto \ln^2 (s/m^2)$. The effective singularity in a complex angular momentum plane which corresponds to this sum at $t = 0$ turns out to be at $j = 1$. The contribution of this singularity to the amplitude will be called a "Froissaron". In the impact parameter representation at $(\ln s/m^2)\cdot\Delta \gg 1$ it is a disk



with constant transparency and with a radius increasing proportionally to $\xi = \ln s/m^2$. In the graph language a Froissaron can be represented by the exchange by a Pomeron bunch. As is shown below, the essential number k of Pomerons in the bunch grows with increasing energy as $(s/m^2)^{\Delta} / \ln(s/m^2)$.

The summation of the enhanced graph contribution to the amplitude at asymptotically high energies again leads to the s-channel unitarity problem. It has been considered for the first time by Bronzan[12]) and Cardy[13]). Cardy has noted that after summing up the eikonal type Pomeron exchanges inside each link of the enhanced graph it is possible to reduce the sum of these graphs down to a set of graphs built of Froissarons (Cardy calls them "superpropagators"). He has shown that the use for the Froissaron a representation of a disk with a sharp edge results in the total cancellation of a enhanced Froissaron graph contribution to the amplitude. As is shown below, for a more realistic form of the Froissaron this Cardy's compensations are not complete. This leads again to the problem of the s-unitarity of the sum of all enhanced Froissaron graphs.

In this paper the theoretical scheme with $\alpha_p(0) > 1$ is considered. Some results have been published previously[14,15]).

The paper is organized as follows. Section 2 presents the consideration of the energy dependence of different physical quantities and only nonenhanced graphs are taken into account. Such an approximation may be valid because of the suppression of the enhanced graph contribution at accessible energies due to the experimental smallness of the Pomeron interaction constants. Taking into account the enhanced graphs does not change qualitatively the results in the asymptotic high energy region.

The expressions for the total, inelastic and elastic cross sections and the ratio of the real-to-imaginary parts of the amplitude are obtained and discussed. It is shown that in the theory with $\alpha(0) > 1$ it becomes possible to explain the so-called geometrical scaling (GS) which has been observed experimentally in pp-scattering. It will disappear with energy increasing, however, at ultrahigh energies. But when $\xi\Delta \gg 1$, GS will be valid again.

The processes of particle production are considered in detail. It is shown that at $\alpha(0) > 1$ the inclusive spectra have a plateau in the central rapidity region with a height which grows as the power of energy. The energy conservation sum rule is not violated becuase the length of the plateau is shorter than the total rapidity interval. The mean multiplicity of produced particles increases also as the power of energy, when $\xi\Delta \gg 1$.

In Section 3 the summation of the enhanced Gribov-Cardy graphs is given and the s-channel unitarity problem is considered. It is found there that Cardy's procedure for summing up Froissaron graphs does not provide the validity of the s-channel unitarity condition. The new method for classifying and summing up graphs is proposed. It yields the integral equation for the contribution of the total graph sum to the scattering amplitude. It has a solution in a form of the Froissaron. The existence of this solution proves the s-channel unitarity condition. So far as the value of $\alpha(0)$



which corresponds to the exact Green function it is smaller than the initial Pomeron intercept shift, the total effects of all enhanced graphs are reduced to the $\Delta \to \Delta_0$ renormalization. It is interesting to note that this phenomenon would appear at energies which are much higher than the asymptotical ones for unenhanced graphs. At these ultrahigh energies the change of the asymptotic region would take place and the growth rate of the total cross section with energy increasing becomes slower. It is not excluded at all that $\Delta_0 \leqslant 0$. In this case the new regime would be not the Froissaron-like one.

## 2. The Growth of the Cross Sections, the Diffraction Cone Slope and Particle Production in the Theory with $\alpha(0)>1$

In this section we disregard the contribution of all enhanced graphs. On the one hand, this contribution at accessible energies is apparently small and on the other hand, as it will be shown below, the total effect of it leads mainly to the renormalization of the $\Delta$ value, without changing the form of the result obtained here.

### 2.1. The elastic scattering amplitude.

It is convenient to use below the impact parameter representation. The partial scattering amplitude (the profile function) $f(\xi, b) = 1 - e^{2i\delta(\xi,b)}$ is defined by the Fourier transform of the scattering amplitude $M_{AB}(\xi, q_\perp)$ for the particles A and B.

$$f_{AB}(\xi, b) = \frac{2}{i}\int M_{AB}(\xi, q_\perp)\, e^{iq_\perp b}\, \frac{d^2 q_\perp}{2\pi} \,. \tag{1}$$

Here $\xi = \ln(s/s_0)$, $s_0 = 2\, m_N^2$, $b$ is the impact parameter, $q_\perp$ is the transverse component of the momentum transferred. The Pomeron contribution to the scattering amplitude is equal to

$$M_{AB}^{(1)}(\xi, q_\perp) = N_A^{(1)} N_B^{(1)} \exp\left[\xi_1 \Delta - (R^2 + \alpha' \xi_1) q_\perp^2\right], \tag{2}$$

where $\xi_1 = \xi - \frac{i\pi}{2}$, $\alpha(-q_\perp^2) \approx 1 + \Delta - \alpha' q_\perp^2$ is a Pomeron trajectory and $N_A^{(1)}(q_\perp^2) N_B^{(1)}(q_\perp^2) = N_A^{(1)} N_B^{(1)} \exp[-R_{AB}^2 q_\perp^2]$ is a Pomeron residue. The assumption on the exponential $q_\perp^2$ dependence of the Pomeron residue and the linear $q_\perp^2$ dependence of the trajectory is valid in the region of small $q_\perp^2$, e.g., in the region of large $b^2$. This region of $b^2$ will be mainly under consideration below.

The Pomeron contribution $\rho(\xi, b)$ to the amplitude (1) has the following form:

$$\rho(\xi, b) = z \exp\left[-\frac{b^2}{4(R^2 + \alpha' \xi)}\right]. \tag{3}$$

where

$$z = \frac{N_A^{(1)} N_B^{(1)}}{R^2 + \alpha' \xi} e^{\xi \Delta}. \tag{4}$$

For the sake of simplicity we have neglected here a small contribution of the real part of the Pomeron amplitude.

It follows from (3) and (4) that the value of $\rho(\xi, b)$ increases with $\xi$ and can become larger than unity violating the unitarity condition. However, the increasing of the cross sections in different channels increases the shadow effects and leads to the suppression of the amplitude. It is seen for the sum of unenhanced graphs shown in Fig 1. The screaning effect if revealed here in the alternating sign of the different rescattering terms and the total contribution to f $(\xi, b)$ is equal to

$$F(\xi, b) = \sum_{n=1}^{\infty} (-1)^{n-1} G_A^{(n)} G_B^{(n)} \rho^n(\xi, b) \frac{1}{n!}. \tag{5}$$

Here, $G_A^{(n)} = N_A^{(n)} / (N_A^{(1)})^n$ and $G_B^{(n)} = N_B^{(n)} / N_B^{(1)})^n$, where $N_A^{(n)}$ and $N_B^{(n)}$ are the vertices for the emission of n Pomerons by the particles. If $b = \text{const}$ and $\xi\Delta \to \infty$, then $\rho(\xi, b) \propto \exp(\xi\Delta)$ is large and each term in series (5) increases with $\xi$ faster than the previous one. So the large number of $n \sim \rho \sim \exp(\xi\Delta)$ is important in (5). Expression (5) can be obtained from the following Lagrangian density of the Pomeron field $\Psi$ [13]

$$L = L_0 + L_1, \tag{6}$$

where

$$\mathcal{L}_0 = \frac{i}{2}(\Psi^+ \dot{\Psi} - \Psi \dot{\Psi}^+) + \frac{1}{2}\alpha'(\nabla\Psi)(\nabla\Psi^+) - \Psi^+\Psi \cdot \Delta, \tag{7}$$

$$\mathcal{L}_1 = \sum_j \sum_{n=1}^{\infty} \frac{i^{n-1}}{n!} N_{A_j}^{(n)} \left[A_j^+ \Psi^n + (\Psi^+)^n A_j\right]. \tag{8}$$

The first term in (6) describes the free field with the mass $(-\Delta)$. The second one corresponds to the Pomeron particle interaction.

Cardy has shown[13] that the summation in (5) can be fulfilled at large $\xi\Delta \gg 1$, when the vertices $N_A^{(n)}$ have an analytical continuation to the complex values of n, when they have no singularities in the right half of the complex n plane and increase there no faster than $\Gamma(n)$. In this case expression (5) can be represented in the form of the Sommerfeld-Watson integral

$$F(\xi, b) = \int_{\uparrow} \frac{dn}{2i}\, G_A^{(n)} G_B^{(n)} \rho^{n}(\xi, b)\, \Gamma(1-n)\,. \tag{9}$$

The path of integration goes along a vertical axis in the complex n-plane. The integrand has in the right half-plane the only singularity, which is the pole at n = 0. The residue in this pole equals $N_A^{(o)} \cdot N_B^{(o)}$. Consider the case when $\xi\Delta \to \infty$ and $b < 2(\alpha'\Delta)^{1/2}\xi - (\alpha'/\Delta)^{1/2}\ln\xi$. Here $\rho(\xi, b) \gg 1$ and the rest of the integral along the vertical contour decreases as $\rho^{-|\mathrm{Re}\,n|}$, when the contour is shifted to the left. So, here $F(\xi, b) = N_A^{(o)} \cdot N_B^{(o)} =$ const. In the region of $b \gg 2(\alpha'\Delta)^{1/2}\xi$ the value of $\rho(\xi, b) \ll 1$ and $F(\xi, b) \approx \rho(\xi, b) \to 0$ at $\xi\Delta \to \infty$. It means that approximately

$$F(\xi, b) \approx N_A^{(o)} N_B^{(o)}\, \theta(4\alpha'\Delta\xi^2 - b^2), \tag{10}$$

where the small correction $\ln\xi/\xi$ to the bound value $4\alpha'\Delta\xi^2$ of $b^2$ has been disregarded.

It follows from (10) that at all $\xi$ $F(\xi, b) \leq 1$ when $N_A^{(o)} \cdot N_B^{(o)} \leq 1$. It means that the unitarity condition is valid at $N_A^{(o)} \cdot N_B^{(o)} \leq 1$ due to shadow effects. Cardy's result (10) means that the factorization takes place in the asymptotic region. In the eikonal approximation $N_A^{(n)} = (N_A^{(1)})^n$, or $G_A^{(n)} = G_B^{(n)} = 1$ in (9). Then the sum in (5) can be evaluated for all $\xi$

$$F(\xi, b) \approx 1 - \exp[-\rho(\xi, b)]\,. \tag{11}$$



In the quasi-eikonal approximation[16]) $G_A^{(n)} = C_A^{n-1}$ and $G_B^{(n)} = C_B^{n-1}$, where $C_A \times C_B = C_{AB}$ is the shower enhanced coefficient arising from the diffraction dissociation contribution. In this case $N_A^{(o)} \cdot N_B^{(o)} = 1/C_{AB}$ and $F(\xi, b) \approx \frac{1}{C_{AB}}\left\{1 - \exp[-C_{AB}\rho(\xi, b)]\right\}$. The object with the profile function $F(\xi, b)$ will be called a "Froissaron". The dependence $F(\xi, b)$ on b at $\xi\Delta \gg 1$ is shown in Fig. 2. It is obvious that the profile function of the Froissaron corresponds to the picture of diffraction on a disk with constant transparency and a radius increasing as $\xi$. The edge of a disk is spread in the transition region with a width which can be estimated from the behaviour of $\rho(b, \xi)$ at $b \approx 2(\alpha'\Delta)^{1/2}\xi$

$$\rho(\xi, b) \approx \frac{N_A^{(1)} N_B^{(1)}}{\alpha'\xi} \exp\left[\frac{2(\alpha'\Delta)^{1/2}\cdot\xi - b}{(\alpha'/\Delta)^{1/2}}\right]. \tag{12}$$

In the $(\xi, q_\perp)$ - representation the sum (5), has the well-known form:

$$M(\xi, q_\perp) = i\sum_{n=1}^{\infty} (-1)^{n-1} \frac{z^n}{n \cdot n!} G_A^{(n)} G_B^{(n)} \exp\left\{-q_\perp^2\left[\frac{R^2 + \alpha'\xi_1}{n}\right]\right\}. \tag{13}$$

In the theory with $\alpha(0) > 1$ $z \sim \exp(\xi\cdot\Delta)$, when $\xi \to \infty$. Here the effective number of the terms n is close to z. Therefore, the Froissaron can be considered as a bunch of Pomerons with the effective number of them increasing with energy as $n \sim z \sim \exp(\xi\Delta)$.

It is easy to write down the expressions for the total and total inelastic cross sections

$$\sigma_{tot}(\xi) = \int 2F(\xi,b)\,d^2b = 8\pi(R^2+\alpha'\xi)\,\varphi(z), \tag{14}$$

$$\sigma_{in}(\xi) = \int [2F(\xi,b) - F^2(\xi,b)]\,d^2b = 4\pi(R^2+\alpha'\xi)\,\varphi(2z). \tag{15}$$

Here $\varphi(z)$ is introduced according to

$$\varphi(z) = \int_0^z (1-e^{-\rho})\frac{d\rho}{\rho} = C + \ln z - Ei(-z), \tag{16}$$

where C = 0.5772 is the Euler constant and Ei(-z) is the integral exponential function; $Ei(-z) \longrightarrow 0$ when $z \longrightarrow \infty$.

From (14)-(16) it follows for the ratio of elastic to total cross sections

$$\frac{\sigma_{el}(\xi)}{\sigma_{tot}(\xi)} = \frac{1}{2}\left[1 - \frac{\ln 2 + Ei(-z) - Ei(-2z)}{C + \ln z - Ei(-z)}\right], \tag{17}$$

where $\sigma_{el}(\xi) = \sigma_{tot}(\xi) - \sigma_{in}(\xi)$ is the total elastic cross section. It is seen from (17) that $\sigma_{el}/\sigma_{tot}$ is of the order of $0.2$ at $z \approx 1$ and tends to 1/2 at $z \longrightarrow \infty$. For the transition to the quasi-eikonal approximation it is necessary to make the substitution $z \longrightarrow z \cdot C_{AB}$ in expressions (14) and (17) and to divide these expressions by $C_{AB}$.

The ratio of the real-to-imaginary parts of the forward scattering amplitude has the following form:

$$\varepsilon(\xi) = \frac{1}{2}\pi\frac{d}{d\xi}\ln[\sigma_{tot}(\xi)] = \frac{1}{2}\pi\left\{\frac{\alpha'}{R^2+\alpha'\xi} + \varphi^{-1}(z)\left(\Delta - \frac{\alpha'}{R^2+\alpha'\xi}\right)(1-e^{-z})\right\}. \tag{18}$$



As is shown below, at accessible energies $\alpha'(R^2+\alpha'\xi)^{-1} \approx \Delta$ for pp-scattering. So, the second term in (18) is small and $\varepsilon(\xi) \approx \frac{1}{2}\pi\Delta$. Therefore, at accelerator energies $\varepsilon(\xi)$ is determined mainly by the contribution of a Pomeron and the secondary poles $f$, $\omega$, $\rho$, $A_2$, etc.

Consider also the expression for the diffraction cone slope parameter $B(\xi)$, determined so that at small $|t|$ $d\sigma/dt \approx d\sigma/dt|_{t=0}\exp[t \cdot B(\xi)]$. It follows from (9) that

$$B(\xi) = 2(R^2+\alpha'\xi)\,\chi(z), \tag{19}$$

where

$$\chi(z) = \varphi^{-1}(z)\int_0^z \varphi(x)\frac{dx}{x}. \tag{20}$$

Consider equations (14)-(20) in the regions of accessible and asymptotic energies. It will be useful to remind that the analysis of experimental data on pp-scattering in the FNAL-ISR energy region ($\xi \approx 5\div 8$) has shown that the so-called geometrical scaling (GS) takes place[17,18]. GS means that the partial scattering amplitude $f(\xi,b)$ depends only on the variable $b^2/B(\xi)$, i.e.,

$$f(\xi,b) = f\left(\frac{b^2}{B(\xi)}\right). \tag{21}$$

The Froissaron contribution to the partial amplitude will satisfy GS when $z$ does not depend on $\xi$ †. This requirement can be satisfied only approximately by the special choice of parameters when at some point $\xi = \xi_0$ the equality $dz/d\xi|_{\xi=\xi_0} = 0$ holds. Together with equation (4) it implies

$$\Delta = \frac{\alpha'}{R^2 + \alpha'\xi_0} . \qquad (22)$$

The use of existing experimental data on the total cross section and the diffraction cone slope for pp-elastic scattering makes it possible to obtain the value of the parameters $\Delta$, $\alpha'$ and $R^2$. It follows from equations (22) and (14) that at $z \approx$ const the growth rate of the total cross section equals

$$\frac{d}{d\xi} \ln \sigma_{tot}(\xi) = \Delta . \qquad (23)$$

As it has been noted in the Introduction, the experiment gives for this rate the value of the order of 6%, i.e.,

$$\Delta \approx 0.06 , \qquad (24)$$

while at accessible energies $\chi(z) \approx 1$ in expression (19) and $B(\xi_0) \approx 10 (\mathrm{GeV}/c)^{-2}$ it follows from (22)-(24) that

$$\alpha' \approx \frac{1}{2} B(\xi_0)\Delta \approx 0.3 \ (\mathrm{GeV}/c)^{-2} . \qquad (25)$$

Putting $\xi_0 = 6$ in expression for $B(\xi_0)$ yields

† Equation (3) has been obtained when $N_A^{(1)}(q_\perp^2)$, $N_B^{(1)}(q_\perp^2)$ depend on $q_\perp^2$ exponentially. It is valid for small $q_\perp^2$ or large $b^2$. In the region of large $q_\perp^2 \gtrsim 1 \ (\mathrm{GeV}/c)^2$ the exponential dependence of the residue seems to contradict experimental data. However, at large $q_\perp^2$, the accuracy to which GS is valid, is not good.



$$R^2 \approx \frac{1}{2} B(\xi_0) - \alpha'\xi_0 \approx 3,2 \ (\mathrm{GeV}/c)^{-2} . \qquad (26)$$

These parameter values are very close to the results which have been obtained by A.M.Lapidus, V.I.Lisin, P.E.Volkovitsky and one of the authors (K.A.T.-M.) from the detailed analysis of experimental data.

It is worth noting that for $\pi p$ and $Kp$ elastic scattering at the same energy $B(\xi) \approx 8 (\mathrm{GeV}/c)^{-2}$, so $R^2 \approx 2.2 \ (\mathrm{GeV}/c)^{-2}$ and is smaller than for pp-scattering. For this reason, meson-nucleon scattering GS should not be so precise as pp and will appear at higher energies

$$\xi_0^{\pi p} = \frac{1}{\Delta} - \frac{R^2_{\pi p}}{\alpha'} \approx 9 . \qquad (27)$$

Thus, in the accessible energy region $z$ remains nearly constant and cross sections and slope parameters increase with energy almost linearly on $\xi$. So the ratios $\sigma_{tot}(\xi)/B(\xi)$, $\sigma_{el}(\xi)/B(\xi)$ and $\sigma_{el}(\xi)/\sigma_{tot}(\xi)$ remain constant. At very high energies, when $\xi\Delta \gg 1$ the cross sections and slope parameters will behave in a universal way

$$\sigma_{tot}(\xi) = 8\pi\alpha'\Delta\xi^2 = 8\pi B(\xi) = 2\sigma_{el}(\xi) . \qquad (28)$$

It is interesting to note that at $\xi\Delta \gg 1$ GS appears once again and becomes exact in accordance with the general result of ref.[19]).

The energy dependence of $\sigma_{tot}(\xi)$ calculated from equation (14) is shown in Fig. 3. At $s \approx 10^9 \ \mathrm{GeV}^2$, where cosmic ray data exist , $\sigma_{tot}$ in pp collisions becomes as large as 100 mb. The authors of ref.[20]) have calcualted the inelastic total cross section $\sigma_{in}$( p- air) with the mean value of $\bar{A}$ =14.4 in the framework of the Glauber model and came to the conclusion that the increase of the pp total cross section, as given by eq. (14), is in contradiction with experimental data on $\sigma_{in}(p\text{-air})$. However, it is necessary to note that the Glauber model is not valid at such a high energy[21]) because at $s \approx 10^9$ GeV$^2$ the transverse dimension of a parton cloud becomes comparable with the nuclear radius. So it is impossible to consider nucleons in nuclei as separate scattering centres, since nucleon parton clouds become strongly overlapped. At ultrahigh energies the Froissaron radius will be larger than nuclear dimension and the effective number of interacting nucleons in nuclei will be equal to unity implying $\sigma_{in}(p\text{-air}) = \sigma_{in}^{pp}$ . It is a consequence of the universal value of $\sigma_{tot}$ in eq. (28) independent of the nature of interacting particles. This strongly contradicts the Glauber model, leading to $\sigma_{in}(p\text{-air}) \approx \bar{A}^{2/3}\sigma_{tot}^{pp}$ even in the case if $\sigma_{tot}^{pp} \to \infty$ .

2.2. The Multiparticle Production

Now turn to particle production processes and consider the inclusive spectra of particles produced in the central region. It follows from the theorem of Abramovsky, Gribov, and Kanchely (AGK)[11]) thatthe onlydiagram which gives a contribution to the inclusive spectra is the cut pole graph, Fig. 3. At $\alpha(0) > 1$ it yields



the inclusive cross section growing as the power of energy

$$\frac{d\sigma}{dy} = 8\pi N_A^{(1)} \cdot N_B^{(1)} \cdot d \cdot e^{\xi\Delta} . \qquad (29)$$

The vertex $d$ is shown in Fig. 4. From equation (29) it follows that the inclusive spectra have a plateau in the central region and that the Feynman scaling is violated.

As has been noted previously[11]), equation (29) contradicts the energy conservation sum rule

$$\frac{1}{\sigma_{in}} \int_0^{\lambda\cdot\xi/2} e^{y} \frac{d\sigma}{dy} dy < e^{\xi/2} . \qquad (30)$$

Here and below we sue the c.m. frame.

If one chooses the upper limit of integration in (30) very close to the edge of the spectrum $1-2\Delta < \lambda < 1$ , inequality (30) is really violated. This result seems to be surprising because the violation of the energy conservation law has not been included in calculations. The solution of this paradox is in fact that eq.(29) is not valid in the whole region of integration. At the edges of the spectrum the Kanchely-Mueller graph (Fig. 4) does not reflect the contribution of the sum of graphs in Fig. 5 in a proper way. Really in the graphs in Fig. 5 with k cut Pomerons the total energy is divided between them mainly in equal parts. Therefore, particles in each cut Pomeron are produced in the rapidity interval of the oder of $\xi - 2\ln k$ . Now find the mean number of cut Pomerons $\langle k \rangle$ in Fig. 5. The cross section $\sigma_k$ of the k-cut Pomeron production is equal to [22])

$$S_k = \frac{4\pi(R^2+\alpha'\xi)}{k}\, e^{-2z}\sum_{m\geq k}^{\infty}\frac{(2z)^m}{m!} = 4\pi(R^2+\alpha'\xi)\,\frac{\gamma(k,2z)}{(k+1)!}\,, \qquad (31)$$

where $\gamma(k,2z)=\int_0^{2z} e^{-x}x^{k-1}dx$ is an incomplete $\Gamma$-function. It gives for a mean value $\langle k\rangle$ :

$$\langle k\rangle = \sum_{k=0}^{\infty} k\, S_k/\sigma_{in} = \frac{2z}{\varphi(2z)} \approx \frac{2N_A^{(1)}N_B^{(1)}}{\alpha'\Delta}\,\frac{e^{\xi\Delta}}{\Delta} \qquad (32)$$

Therefore, the rapidity interval where particles are produced from the cut Pomeron, is equal to $\xi - 2\ln\langle k\rangle = \xi(1-2\Delta)$. It means that the inclusive spectrum can be presented in the form of (29) not in the whole region $|y|<\xi/2$ but only for $|y| < \xi(1/2 - \Delta)$. This corresponds to the value $\lambda = 1-2\Delta$ in the upper limit of the integral (30), satisfying inequality.

Consider now the shape of the inclusive $d\sigma/dy$ spectrum near its edge $|y| \geq \xi(1/2 - \Delta)$. The energy conservation law permits the production of Pomeron showers of the length $2|y|$ in the amount of

$$k_0(y) = \exp\left[\tfrac{1}{2}(\xi - 2|y|)\right]. \qquad (33)$$

This equation taking into account (31) and (32) implies for the average number of showers with the length of $2|y|$ or larger

$$\langle k(y)\rangle = \frac{1}{\sigma_{in}}\sum_{k=1}^{k_0(y)} k\, S_k = \frac{2z}{\varphi(2z)}\, e^{-2z}\left\{\sum_{m=1}^{k_0(y)}\frac{(2z)^{m-1}}{(m-1)!} + \sum_{m=k_0(y)+1}^{\infty}\frac{k_0(y)}{m!}(2z)^{m-1}\right\}. \qquad (34)$$



The sums in brackets in eq.(34) have the following properties: at $(k_0(y)-2z) \gg 2z$ the contribution of the second term is small and the first term is equal to $\exp(2z)$. When $(2z - k_0(y)) \gg 2z$ the main contribution comes from the second term which is reduced to $k_0(y)\exp(2z)/2z$. It implies, taking into account eqs. (33), (34), that eq.(29) for inclusive spectra is valid only at $|y| < y_0 - \delta y_0$, where

$$y_0 = \tfrac{1}{2}\xi - \ln(2z), \qquad (35)$$

$$\delta y = (2z)^{-1/2}. \qquad (36)$$

In the region of $|y| > y_0 + \delta y_0$ expression (29) for the inclusive spectrum acquires the additional factor $\exp(y_0 - |y|)$. Both the curves map together at $y \approx y_0$ with the transition region width $2\delta y_0$ which becomes narrower when energy increases as it follows from eq.(34). In the asymptotic high energy region the spectrum slope shown schematically in Fig. 6 has a break at $y=y_0$. Having the spectrum we can obtain an expression for the average multiplicity $\langle n\rangle$ of particles produced

$$\langle n\rangle = (c+d\xi)\frac{2z}{\varphi(2z)} \underset{\xi\Delta\gg 1}{\approx} 2d\,\frac{N_A^{(1)}N_B^{(1)}}{\alpha'\Delta}\,\frac{e^{\xi\Delta}}{\xi}\,. \qquad (37)$$

Thus, at available maximal energies the inclusive spectrum (29) must have a plateau in the central region of rapidity. The height of this plateau increases as $\exp(\xi\Delta)$ violating the Feynman scaling. Nevertheless, at accessible energies mean multiplicity (37) does not deviate from an ordinary linear dependence because the increase of the plateau is compensated by the growth of inelastic cross section . At higher energies the average multiplicity must increase with energy faster, as is seen from Fig. 7.

Due to the contribution of secondary poles the described picture for inclusive spectra changes significantly now. The value of $\xi \gtrsim 10$ is needed for the Reggeon contribution to become negligible in the centre of the inclusive spectrum.

Now consider briefly the problem of topological cross sections. At accessible energies the experimental data show the existence of the KNO-scaling[23]), which means that

$$\sigma_n = \frac{\sigma_{in}}{\langle n\rangle}\,\Psi\left(\frac{n}{\langle n\rangle}\right).$$

where $\Psi(x)$ is some energy-independent function. Let us neglect the fact that the total energy is divided between produced showers and assume that each shower has on average $\alpha\xi$ particles. Then eq. (31) yields[15]) for $\langle n^{\ell}\rangle$ the following expression

$$\langle n^{\ell}\rangle = (\alpha\xi)^{\ell}\,\Phi_{\ell}(2z)\,, \tag{38}$$

where $\Phi_{\ell}(2z) = (\sigma_{in})^{-1}\sum_{k=1}^{\infty} k^{\ell}\sigma_k$.

It means that in the energy region where $z \approx \mathrm{Const}$, the value of $M_{\ell} = \langle n^{\ell}\rangle/\langle n\rangle^{\ell}$ is energy-independent and leads to the KNO-scaling, with $M_{\ell} = \int_0^{\infty} x^{\ell}\,\Psi(x)\,dx$ .

So the theoretical scheme with $\alpha(0) > 1$ yields the KNO-scaling in the energy region where $z \approx$ const.



Shabelsky and one of the authors of the present paper (K.A.T.-M.) have calculated topological distributions in the framework of the eikonalized Pomeron theory with $\alpha(0) > 1$. (See also,ref.[22]).

The Poisson distribution over the number of produced particles in ladders forming Pomerons was assumed and the division of the total energy between different Pomerons was taken into account. As a result, good correspondence to experiment has been obtained. The theory gives good description of the effect of the appreciable broadening of multiplicity distribution with energy which is observed in experiment. In the theory it occurs due to the contribution of the simultaneous production of several multiperipheral particle showers, that is, the cut Pomeron lines (the so-called "combs"). As has been discussed above, in the accessible energy region the theory yields an approximate KNO-scaling.

At ultrahigh energies a number of peaks emerge in the theoretical curve for the multiplicity distribution. They are due to the diffraction production and to the production of one or more multiperipheral showers[11]).

The picture of multiplicity distribution with the number of peaks appearing at very high energies ($E \gtrsim 10^{8}$ GeV) strongly violates the KNO scaling.

## 3. Enhanced Graphs

### 3.1. The Summing up of Gribov-Cardy's Graphs.

Let us take now into account the interaction between Pomerons. The simplest graphs containing only one interaction vertex are shown in Figs. 8a) and 9a). We assume that similar to the verteces $N_A^{(n)}$, $N_B^{(n)}$, the transition vertex $g_{mn}$ connecting m Pomerons with n ones, has the eikonal from $g_{mn} = g_{oo} g_1^{m+n}$ or, more general, that it permits the single-valued analytical continuation $g_{nm} = g(n,m)$ to the complex m and n planes. Then the sum of the graphs in Fig. 8a (9a) may be substituted by the Froissaron graph shown in Fig. 8b(9b) with the coupling constant $g_{oo} = g(0,0)$. This enables us to pass from the Pomeron graphs to the summation of graphs made up on Froissarons, ref.[13]).

It is necessary to note, however, that graphs with n = m = 1 are included in the sums in Figs. 8a and 9a, although they formally do not exist according to the form of the initial Lagrangian .Indeed, they contain the vertex $g_{11}$ of the transition of one Pomeron into a Pomeron. The corresponding contribution to the Lagrangian $g_{11}\psi^+\psi$ has a form of a mass term and was already included in the free Lagrangian (7) $L_o$ . Nevertheless, we can use the Pomeron interaction Lagrangian

$$L_2' = \sum_{m,n=1}^{\infty} \frac{g_{mn}}{m!\,n!}\, i^{m+n+2} (\psi^+)^m \psi^n \qquad (39)$$

containing this term and corresponding to Figs. 8,9 if the total Lagrangian is redefined as the sum

$$L = L_o' + L_1 + L_2'$$



with $L_o' = L_o - g_{11}\psi^+\psi$ and $L_o$, $L_1$ given by eqs.(7) (8). It is just similar to the use of $L_o$ as a free Lagrangian and having no term $g_{11}\psi^+\psi$ in the interaction part $L_2 = L_2' - g_{11}\psi^+\psi$ .
The use of $L_o'$ instead of $L_o$ corresponds to the redefinition in (7) $\Delta \to \Delta_o$ , where

$$\Delta_o = \Delta - g_{11} \qquad (40)$$

Thus, the account of the enhanced Pomeron graph contribution leads to the enhanced Froissaron graphs of the type shown in Figs. 8,9, where $F_o$ is a Froissaron and $\rho_o$ corresponds to the Pomeron (with $\Delta$ substituted by $\Delta_o$ ).

In the accessible energy region the enhanced graphs contribution is actually small due to the smallness of the Froissaron coupling constant $g_{oo}$ ( or of the vertices $g_{mn}$ of the Pomeron coupling). However, in the far asymptotic region enhanced graphs could be essential as their contribution grows with energy so fast that each of them separately violates unitarity. For instance, the singularity $\omega^{-6}$ in the ( $\omega$ , $q_\perp$ ) representation corresponds to the graph in Fig. 8b. Its contribution to $\sigma_{tot}(\xi)$ is proportional to $\xi^5$ at $\xi \to \infty$ ).

The s-unitarity for the sum of enhanced graph contributions has been analysed by Cardy[13]). He has noted that there is a complete cancellation, in approximation (10) of the contribution of Froissaron graphs in Figs. 8b and 9b . Their sum is equal to the value corresponding to the graph shown in Fig. 8b multiplied by the factor

$$1 - \theta( a_o^2 \xi^2 - b^2 ), \qquad (41)$$

where

$$a_o^2 = 4\alpha'\Delta_o \,. \tag{42}$$

The sum is zero as with $b^2 > a_o^2 \cdot \xi^2$ the contribution of the graph in Fig. 8b is itself proportional to $\theta\,(a_o^2 \cdot \xi^2 - b^2)$. Since the factor $\theta(a_o^2 \cdot \xi^2 - b^2)$ corresponds to any additive Froissaron line then there is always a similar complete compensation of enhanced Froissaron higher order graph contributions in each order in $g_{oo}$. So far the summation over all Froissaron graphs yields only one $F_o$ contribution which is unitary in the s channel.

However, a bit more accurate calculation taking into account a small deviation of the Froissaron profile from the $\theta$-function, shows [15]) that the above compensations are not complete and do not at all guarantee the unitarity. There are two reasons why the $\theta$-function approximation is crude. At first, the account of the smearing out at the edge of the Froissaron disk, shows that the unitarity is violated at each stage of Cardy's summation procedure. Consider, for example, the graph 8b contribution to the partial amplitude at the distances

$$b = 2\,(\alpha'\Delta_o)^{1/2}\,\xi - (\alpha'/\Delta_o)^{1/2}\ln\xi \,. \tag{43}$$

Let $b_1$ and $y$ be an impact parameter and rapidity corresponding to the vertex $g_{oo}$. With $b_1 \approx a_o y$ eqs. (3), (4) and (9) imply $F_o\,(y,\, b_1) \propto 1/y_1$. At the same time, the second Froissaron in Fig. 8b yields the contribution $F_o\,(\xi - y\,,\, |b - b_1|) = \mathrm{const}$ for $b_1$ displayed in the crossing region of both the disks. The area of this region is proportional to $\xi^{1/2}$. So, after integrating over $b_1$ and $y$, the contribution of the diagram in Fig. 8b will rise as $\xi^{1/2}$ at the impact parameter values of the order of (43). Small compensation which occurs after the addition of the graph in Fig. 9b does not change the result because $1 - F_o\,(\xi,\, b) = \mathrm{const}$ due to condition (43). So, the s-channel unitarity for the partial amplitude is violated even in this simplest case.

There is another reason also leading to the contribution with the unitarity when a more realistic form of $F_o(\xi\,,\, b)$ rather than (10) is used. A small distinction $F_o\,(\xi\,,\, b)$ from unity at $b < a_o\xi$ is important. Let us call those graphs irreducible in the s-channel which cannot be divided by a vertical line into two parts without crossing the Pomeron lines or vertices $g_{mn}$. Let $G\,(\xi\,,\, b)$ be the contribution of such a graph differing from $\rho_o(\xi\,,\, b)$-Pomeron contribution, for example, the contribution of the graph in Fig. 8. For a given graph there will be graphs generated by the iteration of $G(\xi, b)$ in the s-channel. Let us denote the sum of such iterations by the symbol $E\,\{G(\xi, b)\}$. In the eikonal approximation, e.g., it is equal to

$$E\{G(\xi, b)\} \approx 1 - \exp\{G(\xi, b)\} \,. \tag{44}$$

Suppose that $G(\xi, b) < 0$ and that $G\,(\xi, b)$ is an exponentially increasing function of $\xi$. As is shown below, just this case is a real one for graphs with the form of a chain of the type shown in Fig. 8. Consider what may happen in the limit $\xi \to \infty$. In the same eikonal approximation the rescatterings via a Froissaron give (44) the screening factor

$$\exp\{-\rho_0(\xi,b)\} \qquad (45)$$

rather than (41). It is clear now that there can be two different cases at $G(\xi,b)<0$: (i) if $|G(\xi,b)| < \rho_0(\xi,b)$ in the limit $\xi \to \infty$, then the unitarity will be conserved, or otherwise (ii) if $|G(\xi,b)| > \rho_0(\xi,b)$, then it will be crudely violated.

Thus, the problem of the s unitarity of the theory can be solved only after the summation over all enhanced Froissaron graphs. The method to solve both the problems has been developed in ref.[14])

The main idea was to consider the elastic scattering amplitude $f_{AB}(\xi,b)$ shown in Fig. 10, as a sum of the s-channel eikonal type iterations of the contributions $\upsilon(\xi,b)$ of all irreducible (in the s-channel) graphs

$$f_{AB}(\xi,b) = N_A^{(0)} N_B^{(0)} f(\xi,b) \qquad (46)$$
$$f(\xi,b) = E\{\upsilon(\xi,b)\}$$

It fulfills obviously the s-channel unitarity condition $|f| \leq 1$ if $\upsilon(\xi,b)$ is positive for any $\xi$ and $b$.

To investigate the latter problem let us construct an equation for the exact amplitude $f(\xi,b)$. For this purpose we divide the graphs contributing to $\upsilon(\xi,b)$ into three classes: the Pomeron function $\rho_0(\xi,b)$ and two groups denoted by $D(\xi,b)$ and $C(\xi,b)$ as is shown in Fig. 11, that is $\upsilon(\xi,b)$ will be written in the following way:

$$\upsilon(\xi,b) = \rho_0(\xi,b) + \mathcal{D}(\xi,b) + C(\xi,b) \qquad (47)$$



The group D contains the graphs irreducible both in the s-channel and t-channel. These graphs cannot be divided by a horizontal line without crossing Pomeron lines. It is clear that after all possible summations and reductions within these graphs, the group D turns into a series of Gribov's graphs[6]) built up of exact Green functions $f(\xi,b)$ (46) and the vertices $g_{00}$. Each of these vertices couples three or more lines $f(\xi,b)$. Some simple examples are presented in Fig. 11.

The totality of graphs from the group C form the t-channel chains with the number of links not smaller than two. Each link Z is a sum of graphs which cannot be divided by a horizontal line, crossing only the Pomeron interaction vertices. At the same time unlike the group D these graphs can be reducible in the s-channel. For these reasons one can write $Z(\xi,b)$ as

$$Z(\xi,b) = f(\xi,b) - C(\xi,b)\,. \qquad (48)$$

On the other hand, C is easily expressed through Z if one looks at Fig. 11 and passes to the $(\omega, q_\perp)$ representation.

$$C(\omega,q_\perp) = Z(\omega,q_\perp)\sum_{n=1}^{\infty}\left[g_{00}Z(\omega,q_\perp)\right]^n =$$
$$= \frac{g_{00}Z^2(\omega,q_\perp)}{1-g_{00}Z(\omega,q_\perp)}\,. \qquad (49)$$

$C(\omega,q_\perp)$ can be found from (48) and (49)

$$C(\omega,q_\perp) = \frac{g_{00}f^2(\omega,q_\perp)}{1+g_{00}f(\omega,q_\perp)}\,. \qquad (50)$$

It is clear now that the sum of the graphs shown in Fig. 12 corresponds to expression (50).

So, the right-hand part of (46) can be expressed through the function $f(\xi, b)$. Consequently, relation (46) has a form of an integral equation for the amplitude $f(\xi, b)$. As a possible solution of this equation one can consider the Froissaron $F_o$ .

$$f(\xi, b) = F_o(\xi, b) \approx \theta(a_o^2 \xi^2 - b^2) \quad . \tag{51}$$

After substituting (51) into the graphs of the group D (f) large Cardy's compensations take place.

The only remaining graph in the group D is the simplest one. with two vertices $g_{oo}$ . Its contribution is large and positive for $b < a_o \xi$ and is equal to zero at $b > a_o \xi$ .

The consideration of the graphs from the class C(f) is more complicated. At the impact parameters $b > a_o \xi$ the contribution of these graphs is equal to zero. Let us consider the case of $b < a_o \xi$ and pass to the $(\omega, q_\perp)$ representation. It is convenient to rewrite (50) in the following way:

$$C(\omega, q_\perp) = f(\omega, q_\perp) - \left[ f^{-1}(\omega, q_\perp) + g_{oo} \right]^{-1} . \tag{52}$$

Froissaron (51) in the $(\omega, q_\perp)$ representation has a form of

$$F_o(\omega, q_\perp) = a_o^2 (\omega^2 + a_o^2 q_\perp^2)^{-3/2} . \tag{53}$$

Since the first term in (52) is positive, concentrate our attention at the second one. After substituting (53), it is equal to



$$C(\omega, q_\perp) - f(\omega, q_\perp) = \frac{-a_o^2}{(\omega^2 + a_o^2 q_\perp^2)^{3/2} + \tilde{g}_{oo}} , \tag{54}$$

where $\tilde{g}_{oo} = a_o^2 g_{oo}$ . This expression in the case of $g_{oo} > 0$ has two poles in the right $\omega$-half plane:

$$\omega_{1,2} = \left[ \eta_{1,2} \tilde{g}_{oo}^{2/3} (q_\perp^2) - a_o^2 q_\perp^2 \right]^{1/2} \tag{55}$$

$$\eta_{1,2} = \exp(\pm \tfrac{1}{3} i \pi)$$

If $g_{oo} < 0$, then only one pole with $Re\,\omega > 0$ exists:

$$\omega_1 = \left[ |\tilde{g}_{oo}(q_\perp^2)|^{2/3} - a_o^2 q_\perp^2 \right]^{\frac{1}{2}} . \tag{56}$$

At $\xi \to \infty$ the pole term gives the main contribution to $C(\xi, q_\perp)$ , which for $g_{oo} > 0$ is equal to:

$$C(\xi, q_\perp) \approx -\frac{2}{3} Re \frac{a_o^2 \exp\{(\tilde{g}_{oo}^{\frac{2}{3}} \eta_1^2 - a_o^2 q_\perp^2)^{\frac{1}{2}} \xi\}}{\tilde{g}_{oo}^{\frac{1}{3}} \eta_1 (\tilde{g}_{oo}^{\frac{2}{3}} \eta_1^2 - a_o^2 q_\perp^2)^{\frac{1}{2}}} . \tag{57}$$

If $g_{oo} < 0$, then

$$C(\xi, q_\perp) \approx -\frac{1}{3} \frac{a_o^2 \exp\{(|\tilde{g}_{oo}|^{\frac{2}{3}} - a_o^2 q_\perp^2)^{\frac{1}{2}} \xi\}}{|\tilde{g}_{oo}|^{\frac{1}{3}} (|\tilde{g}_{oo}|^{\frac{2}{3}} - a_o^2 q_\perp^2)^{\frac{1}{2}}} . \tag{58}$$

The value of $C(\xi, b)$ is obtained from (56), (57) by means of Fourier transform

$$C(\xi, b) = \frac{1}{2\pi} \int C(\xi, q_\perp) e^{-i b q_\perp} d^2 q_\perp . \tag{59}$$

The calculation of this integral is accomodated in Appendix I. It is carried out in the complex $q_\perp$-plane by means of the saddle point method. The result is equal to

$$C(\xi, b) \approx -\frac{2}{3} Re \frac{\theta(a_o^2 \xi^2 - b^2) \exp\{\tilde{g}_{oo}^{\frac{1}{3}} \eta_1 (\xi^2 - \frac{b^2}{a_o^2})^{\frac{1}{2}}\}}{\tilde{g}_{oo}^{\frac{1}{3}} (\xi^2 - b^2/a_o^2)^{\frac{1}{2}}} \tag{60}$$

if $g_{oo} > 0$. In the case of $g_{oo} < 0$

$$C(\xi,b) \approx -\frac{1}{3}\,\frac{\theta(a_o^2\xi^2-b^2)\exp\{|\tilde{g}_{oo}|^{\frac{1}{3}}(\xi^2-\frac{b^2}{a_o^2})^{\frac{1}{2}}\}}{|\tilde{g}_{oo}|^{\frac{1}{3}}(\xi^2-b^2/a_o^2)^{\frac{1}{2}}} \quad (61)$$

Expression (60) oscillates when $\xi$ rises and b is constant. The value of (61) is always negative. So, if one wants the sum (47) to be positive at any value of b and $\xi$, one should impose the following condition

$$|C(\xi,b)| \leq \rho_o(\xi,b) \quad (62)$$

for $b < a_o\xi$. But this inequality is obviously violated near the edge of the Froissaron disk, i.e.,at $b - a_o\xi = \text{const}$. Here $\rho_o(\xi, b) \propto 1/\xi$ decrease with energy increasing but $|C(\xi,b)| \propto \exp(A\xi^{\frac{1}{2}})/\xi$ is a rising function of $\xi$. Nevertheless, it is seen from (57) and (58) that if $\tilde{g}_{oo}(q_\perp)$ depends on $q_\perp^2$ by means of

$$g_{oo}(q_\perp^2) = g_{oo}(0) - \tau^2 q_\perp^2 \quad (63)$$

then the number of $a_o^2$ is substituted by $a^2 - C_o r^2$, where $C_o$ is a constant. So, the $q_\perp^2$ - dependence of $g_{oo}(q_\perp^2)$ is decreasing, i.e., $r^2 > 0$, then $C(\xi, b)$ has a smaller radius in comparison with $\rho_o(\xi, b)$ and condition (62) can be satisfied if

$$\tilde{g}_{oo}(0) < 8\Delta_o^3 \text{ for } g_{oo} > 0$$
$$|\tilde{g}_{oo}(0)| < \Delta_o^3 \text{ for } g_{oo} < 0 . \quad (64)$$

Thus, solution (51) does not contradict the s-channel unitarity. However, this solution is only approximate, because the right-hand side of (46) does not sharply drop to zero when b passes through $b = a_o\xi$, but smoothly decreases as $E\{\rho_o(\xi, b)\}$. There are



some arguments in favour of the unimportance of the smoothing edge. Although the radius of the sum of graphs, which belong to C(f) can rise and be larger than $a_o\xi$ (for $g_{oo} < 0$) it is possible to compensate this by choosing the value of $r^2$ in (63). As for the graphs of the group D, it can be shown that each graph contribution is decreased with energy rising at $b \geq a_o\xi$. This is due to the fact that each of the vertices $g_{oo}$ in the graphs of the group D couples three or more lines. Although the number of selection graphs is infinite, their contributions have alternative signs, and one can assume that the summed up contribution is also decreased with $\xi$ rising at $b > a_o\xi$. In the region of $b < a_o\xi$ the smoothing edge of the Froissaron disk does not play any role, and $D(\xi, b) \propto \exp[-\rho_o(\xi, b)]$ is very small here because of Cardy's compensations.

## 3.2. The renormalization of the $\Delta$-value [15]

Let us draw our attention to the fact that the interaction radius squared, $4\alpha'\Delta_o\xi^2$, corresponding to solution (51) is smaller by $4\alpha' g_{11}\xi^2$ than that which arose above for the unenhanced graphs only. In other words, the enhanced graph contribution is reduced effectively to the renormalization of the $\Delta$-value in accordance with (40). In the energy region of the near future accelerators $\xi \gtrsim 10$ the transition of the total cross section to the Froissart behaviour will begin. But the simplest enhanced graphs shown in Figs. 8b,9b demand the value of $\xi$ two times larger for the asymptotic behaviour. So, at superhigh energies when the cross sections already rise as $8\pi\alpha'\Delta\xi^2$ some slowing-down of the growth rate will take place. This change of the asymptotic regime corresponds to the reduction of the $\Delta$ -value. This situation can be explained by the simplified example, shown in Fig. 13, where only unenhanced graphs and the first enhanced graphs with one vertex $g_{oo}$ are taken into account. Since we use here the Froissaron F, containing the vertex $g_{11}$ contribution, the graphs in Fig. 13c) and e) should be subtracted. At modern energies the contributions of the triple Pomeron graph (which is negative) and more complicated graphs are negligibly small. So, the contributions of the graphs b) and c) (d,e) compensate each other, and the cross sections rise as (14). But in asymptotics the sum of the graphs b) and d) gives a contribution to $\sigma_{tot}$ rising as $\xi^{3/2}$, i.e., small. As for the graphs c) and e), they give the summing contribution $-8\pi\alpha' g_{11}\xi^2$ and decrease the $\Delta$-value.

The same conclusion is valid for the multiparticle production reactions. It is shown in Appendix II that enhanced graph contribution renormalizes the value of $\Delta \to \Delta_o$ in the inclusive cross section of (29) and in the mean multiplicity (37)† and changes also the values of the factor $d$ contained in this expressions. The only exception is the case when a particle is extracted from the cut vertex, as is shown in Fig. 14. The corresponding contribution slightly bends the inclusive spectrum, which is given by the

† If Pomeron interaction is strong enough, then AGK-cutting rules can be violated and the mean multiplicity will rise only as a power of $\xi$. We thank E.M.Levin and M.G.Riskin for their helpful discussions of this problem.



following expression:

$$\frac{d\sigma}{dy} = 8\pi N_A^{(1)} N_B^{(1)} \left[ d_o e^{\xi\Delta_o} + h\, y^2(\xi - y)^2 \right] . \qquad (65)$$

The coefficient $d_o$ is obtained in Appendix II, and the factor $h$ is defined in Fig. 14.

It is interesting to note that a case is not excluded when $g_{11} \geq \Delta$ , or $\Delta_o \leq 0$. The possibility of such a situation is supported by the simple estimation of $g_{11}$ in the one-pion exchange model as is shown in Fig. 15.

After calculations one has

$$g_{11} \approx \frac{(\sigma_{tot}^{\pi N})^2}{16\pi^3 \sigma_{tot}^{NN}} \left[ R_1^{-2} - 2\mu^2 \ln(\mu^2 R_1^2) + \mu^2 \right] , \qquad (66)$$

where $\mu$ is the pion mass; $R_1^2/2$ describes the dependence of $\sigma_{tot}^{\pi N}$ on the virtual pion mass squared. If one puts $R_1^2 = 1/(\mathrm{GeV}/c)^{-2}$, then one finds from (66) $g_{11} \approx 0.08$, which is of the same order as $\Delta$ .

If the case of $\Delta_o \leq 0$ is realized, then the Froissart-like behaviour is not possible. This is seen from equations (46)-(47) which are valid as earlier. The negative value of $C(\xi, b)$ cannot be compensated by anything now, because $\rho_o(\xi, b) \to 0$ as $\xi \to \infty$. Consequently, the solution $F_o(\xi, b)$ is not suited here and the total cross sections will rise asymptotically not faster than

$$\sigma_{tot}(\xi) \propto \xi^{\eta} , \qquad (67)$$

where

$$\eta < 2 \qquad (68)$$

So after the change of the asymptotic regime at superhigh energies the Froissart behaviour can pass to more gentle slope rising. The inclusive cross section and the mean multiplicity in this case are equal to

$$\frac{d\sigma}{dy} \propto y^{\eta}(\xi - y)^{\eta}; \qquad \langle n \rangle \propto \xi^{\eta+1} . \tag{69}$$

It is worth while noting finally that the critical value $\Delta = \Delta_c$ is known for which the strong coupling version occurs[7,24]). In this case the right-hand side of (47) has a singularity with $\mathrm{Re}\,\omega = 0$. So the Froissart-like regime is impossible and the case of $\Delta = \Delta_c$ corresponds to the situation with $g_{11} \geqslant \Delta$ , i.e.,

$$\Delta_c \leqslant g_{11} . \tag{70}$$

This is in agreement with the estimates of $\Delta_c$ from [7]) and $g_{11}$ from (66).

4. Conclusion

The problem of increasing cross sections has been discussed in some papers based on different approaches (see, e.g., ref.[25])). Here we have considered a version of the Pomeron theory with $\alpha(0) > 1$. The value of $\alpha(0)$ has been introduced phenomenologically but it is worth while mentioning that the Pomeron intercept in the field theory is a function of the coupling constant. So, the value of $\alpha(0) = 1$ is not an upper limit and the possibility of $\alpha(0) > 1$ exists[26,27]).

A small displacement of the Pomeron pole position in the j-plane to the right of unity at modern energies leads to a number of subtle corrections to the physical observables, which are needed for the agreement between the theory and the experiment. But in the higher



energy region which will be accessible at future accelerators, the strong interaction theory is absolutely changed. Instead of the Pomeron dominated in the theory with $\alpha(0) = 1$ a new object-Froissaron which is a many Pomeron "stream" determines the high energy behaviour. Below is a short list of the main consequences at accessible and asymptotic energies from the Pomeron theory with $\alpha(0) > 1$.

1. Total cross sections and diffraction slopes rise linearly with $\xi$ in a modern energy region such as the phenomenon of approximate GS takes place. As $\xi$ becomes larger, GS is violated and emerges again in asymptotics when both the cross section and the slope rise as $\xi^2$ .

2. The ratio of elastic-to-total cross sections is small (about 1/5) and constant at modern energies and will be large (about 1/2) in asymptotics.

3. The ratio of the real-to-imaginary parts of the forward scattering amplitude after it becomes positive will reach the value of about $\frac{1}{2}\pi\Delta$ and for a very long heried will remain approximately a constant.

4. The inclusive spectrum has a plateau in the central region. The height of the plateau rises as $\exp(\xi\Delta)$ , violating the Feynman scaling. The rapidity interval of this plateau is only $\xi$ (1 - 2 $\Delta$ ), so the momentum conservation sum rule is satisfied.

5. The mean multiplicity does not obtain any visible corrections at modern energies and rises linearly with $\xi$ . But at the energy of $\xi \gtrsim 20$ significant deviation from the ordinary growth will emerge and asymptotically $\langle n \rangle$ will rise as $\exp(\xi\Delta)/\xi$

6. The KNO-scaling in the topological cross sections can take place at modern energies, but it surely will be violated at higher energies. The multiplicity distribution curve asymptotically will have oscillations.

7. The enhanced graph contribution changes the asymptotic regime at superhigh energies. It renormalizes the value of $\Delta \longrightarrow \Delta_0 = \Delta - g_{11}$. The coordination of the asymptotic behaviour with the s-channel unitarity is proved.

8. In the case of $\Delta \leqslant g_{11}$ the Froissart-like asymptotics is not possible and the cross sections rise slower than $\xi^2$ after changing the asymptotic regime.

Acknowldegements

We are grateful to K.G.Boreskov, A.B.Kaidalov, A.M.Lapidus, E.M.Levin, M.G.Riskin, P.E.Volkovitsky for valuable discussions.



## APPENDIX I

Let us carry out the integration in (59) for the case of $c(\xi, q_\perp)$ given by eq. (57). The case of $g_{oo} < 0$ is analogous.

After integrating in (59) over the angle one obtains

$$C(\xi, b) \approx -\frac{2}{3} \mathrm{Re} \frac{a_o^2}{\tilde{g}_{oo}^{\frac{1}{3}}} \int_0^\infty \frac{\exp\{(\tilde{g}_{oo}^{\frac{2}{3}} \eta_1^2 - a_o^2 q_\perp^2)^{\frac{1}{2}} \xi\}}{(\tilde{g}_{oo}^{\frac{2}{3}} \eta_1^2 - a_o^2 q_\perp^2)^{\frac{1}{2}}} J_o(q_\perp b) q_\perp dq_\perp \; . \tag{I.1}$$

Using the folowing relation:

$$H_o^{(1)}(x) - H_o^{(1)}(-x + i0) = \pm 2 J_o(x) \tag{I.2}$$

one can pass to the expression

$$C(\xi, b) \approx -\frac{1}{3} \mathrm{Re} \frac{a_o^2}{\tilde{g}_{oo}^{\frac{1}{3}}} \int_C \frac{\exp\{(\tilde{g}_{oo}^{\frac{2}{3}} \eta_1^2 - a_o^2 q_\perp^2)^{\frac{1}{2}} \xi\}}{(\tilde{g}_{oo}^{\frac{2}{3}} \eta_1^2 - a_o^2 q_\perp^2)^{\frac{1}{2}}} H_o^{(1)}(q_\perp b) q_\perp dq_\perp \; . \tag{I.3}$$

The path of integration $C = C_o$ is shown in Fig. 16. The same figure shows also the branching points of the expression under the integral in (I.3). Cuts are drawn in such a way that the function $\exp\{(\tilde{g}_{oo}^{2/3} \eta_1^2 - a_o^2 q_\perp^2)^{\frac{1}{2}} \xi\}$ decreases in the upper half-plane as $|q_\perp| \longrightarrow \infty$. From the asymptotic behaviour of the function $H_o^{(1)}(z)$

$$H_o^{(1)}(z) \approx \sqrt{\frac{2}{\pi z}}\, e^{iz - \frac{1}{4} i\pi} \tag{I.4}$$

one can see that the expression under integral in (I.3) decreases in the upper half-plane as $|q_\perp| \to \infty$, so one can change the path of integration from $C_o$ to $C_1$, and to carry out the integration by the saddle point method. The place $q_o$ of the saddle point is determined by the zero condition of the logarithmic derivative from the expression under the integral in (I.3):

$$q_o = \frac{i\eta_1 b}{a_o(a_o\xi - b^2)} \cdot \qquad \text{(I.5)}$$

The motion of $q_o$ in the $q_\perp$-plane with the growth of b is shown in Fig. 16. Using (I.5) and the fact that the expression under the integral (I.3) is exponentially small in the upper part of the contour $C_1$, one can calculate the integral by the saddle point method and obtain the result (60).

It is necessary to note that the denominator in (60) tends to zero as $b \to a_o\xi$. This is due to the fact that the second logarithmic derivative from the under-integral expression in (I.3) is equal to $\ell'' = -a_o^2(\xi - b^2/a_o^2)^{3/2}/(\eta_1\xi^2)$ and tends to zero, but for the saddle point method this derivative should be of the order of $|\ell''| \propto \xi$.



# APPENDIX II

It is shown here that the enhanced graph contribution does not change essentially expressions (27) for the mean multiplicity but only renormalizes the constants $d \to d_o$ and $\Delta \to \Delta_o$.

The inclusive cross section $d\sigma/dy$ corresponds to the Kancheli-Mueller graph which is shown in Fig. 17 in the left-hand side of the AGK graphical equality (one should compare it with Figs. 10-12).

It follows from the AGK-cutting rules for the enhanced graphs that $\widetilde{\mathcal{D}}(\xi, y) = 0$. For this reason

$$\widetilde{f}(\xi) = \widetilde{\rho}_o(\xi) + \widetilde{C}(\xi). \qquad \text{(II.1)}$$

T e notation used here is of the following type:

$$\int_0^\xi \widetilde{\rho}_o(\xi, y)\,dy = \widetilde{\rho}_o(\xi), \qquad \text{(II.2)}$$

i.e.

$$\widetilde{f}(\xi) = \int_0^\xi \frac{d\sigma(\xi,y)}{dy}\,dy = \langle n\rangle \sigma_{in}(\xi). \qquad \text{(II.3)}$$

Now pass in (II.1) to the $\omega$-representation by the transformation similar to

$$\widetilde{C}(\omega) = \int \widetilde{C}(\xi) e^{-\omega\xi} d\xi. \qquad \text{(II.4)}$$

If one sums up the geometrical progressions $\sum_{n=0}^{\infty}(-1)^n[g_{oo}f(\omega,0)]^n$ up and down from the cut link $\widetilde{f}(\omega)$ in $\widetilde{C}(\omega)$, then the following expression for $C(\omega)$ arises:

$$\widetilde{C}(\omega) = -\frac{\widetilde{f}(\omega)}{[1 + f(\omega,0)]^2} + \widetilde{f}(\omega). \qquad \text{(II.5)}$$

The second term here is required because of the absence of a graph with only one link in C. After substituting it into (II.1) one finds

$$\tilde{f}(\omega) = [1 + g_{oo} f(\omega, 0)]^2 \tilde{\rho}_o(\omega). \qquad \text{(II.6)}$$

Remembering that $\rho_o(\omega) = d/(\omega - \Delta_o)^2$ and $f(\omega, 0) = a_o^2/\omega^3$, one obtains at $\omega \to \Delta_o$

$$\tilde{f}(\omega) \approx \left(1 + \frac{\tilde{g}_{oo}}{\Delta_o^3}\right)^2 \frac{d}{(\omega - \Delta_o)^2}. \qquad \text{(II.7)}$$

After passing to the $\xi$ -representation using (II.3) one has

$$\langle n \rangle \sigma_{in}(\xi) = d_o \xi e^{\xi \Delta_o}, \qquad \text{(II.8)}$$

where

$$d_o = \left(1 + \frac{\tilde{g}_{oo}}{\Delta_o^3}\right)^2 \cdot d. \qquad \text{(II.9)}$$

So, the enhanced graph contribution changes $\Delta \to \Delta_o$ in expressions (27,(37) for $\langle n \rangle$ and $d\sigma/dy$, and also gives to these expressions the supplementary factor $(1 + \tilde{g}_{oo}/\Delta_o^3)^2$.



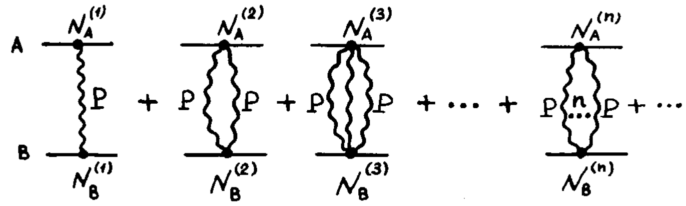


Fig. 1. Unenhanced Pomeron graph series.

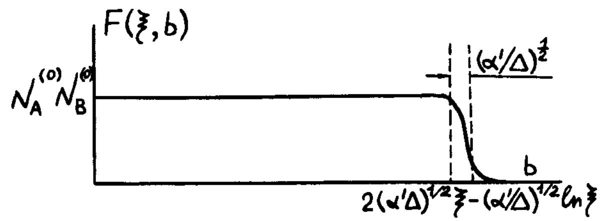


Fig. 2. The profile function corresponding to the Froissaron.

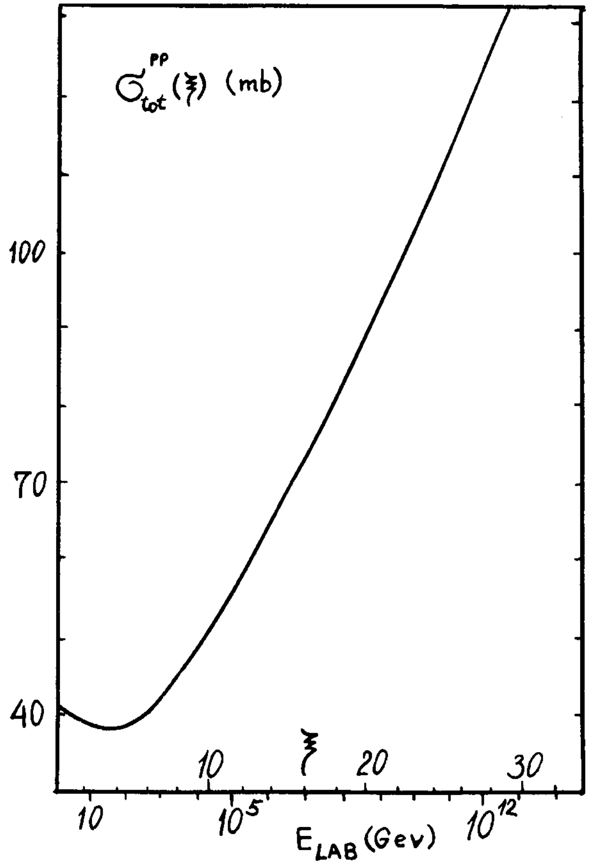


Fig. 3. The energy dependence of $\sigma^{pp}_{tot}$ calculated with (14). The Reggeon contribution is also included.



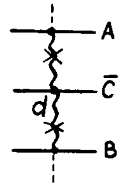


Fig. 4. The Kanchely-Mueller graph for inclusive cross section.

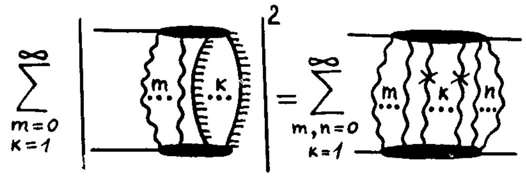


Fig. 5. The sum of cut unenhanced graphs giving contribution to the inclusive cross section.

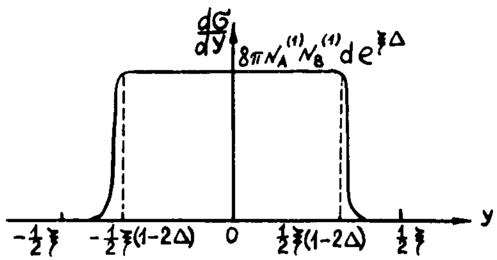


Fig. 6. The asymptotic form of the inclusive spectrum in c.m.s.

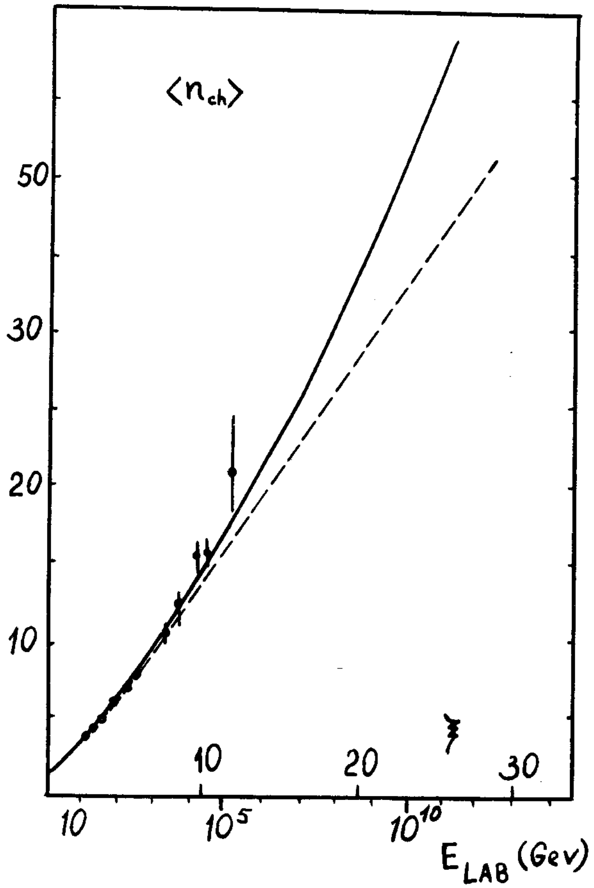


Fig. 7. The energy dependence of charged particle mean multiplicity in pp-collision. —— is n calculated with (37); ---- is a curve from ref.[22]) corresponding to $\alpha(0) = 1$.



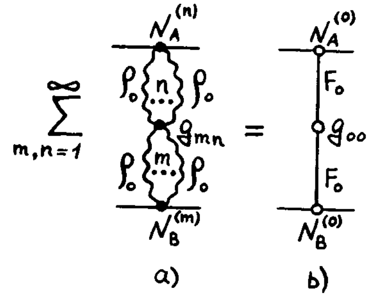

Fig. 8. The simplest enhanced Froissaron graph.

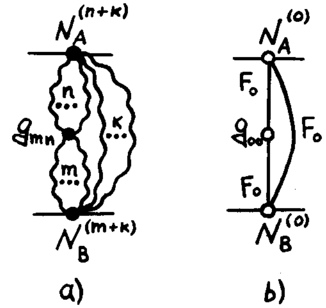

Fig. 9. The enhanced Froissaron graph with rescattering corrections.

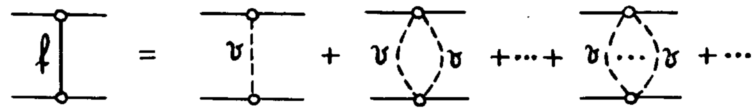

Fig. 10. An example of the eikonalization procedure.

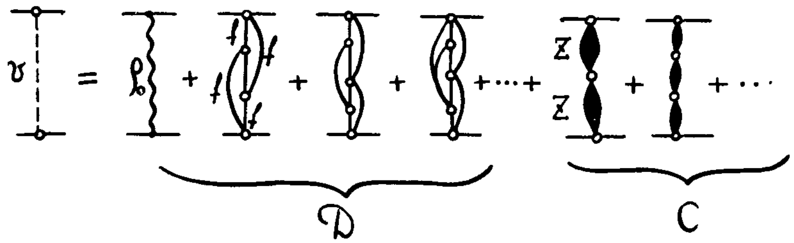


Fig. 11. The classification of the graph irreducible in the $\mathfrak{s}$-channel.

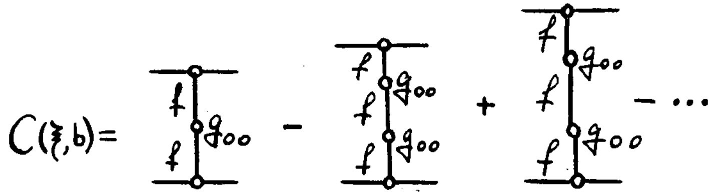

Fig. 12. The connection of C( $\xi$ ,b) with the exact Green function f( $\xi$ ,b) .

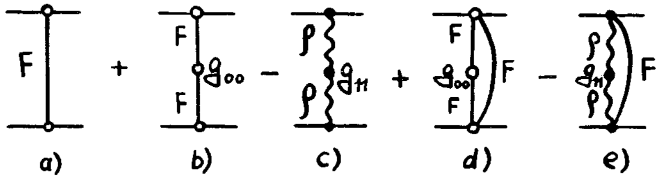


Fig. 13. The simplest enhanced graphs which give the fisrt order in the $g_{oo}$ correction to F( $\xi$,b).



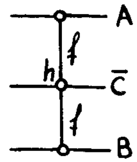


Fig. 14. The Kanchely-Mueller graph with a particle extracted from the cut vertex $g_{oo}$ .

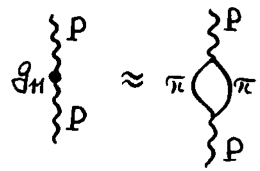

Fig. 15. The pion loop graph for estimating $g_{11}$ .

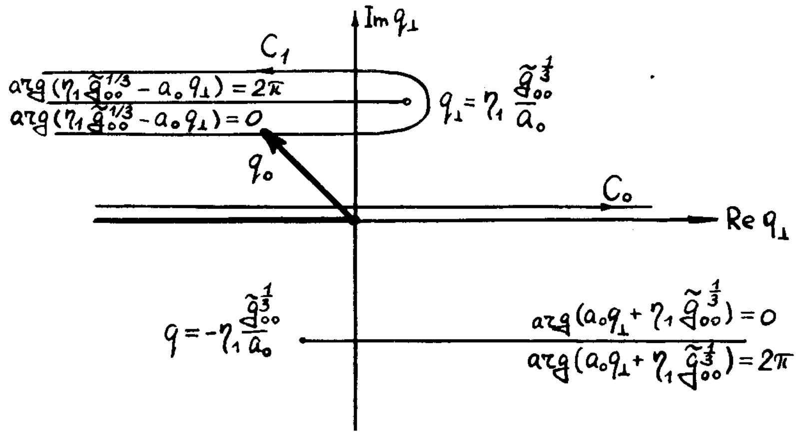


Fig. 16. The complex $q_\perp$-plane with the saddle poits and the integration contour pointed.

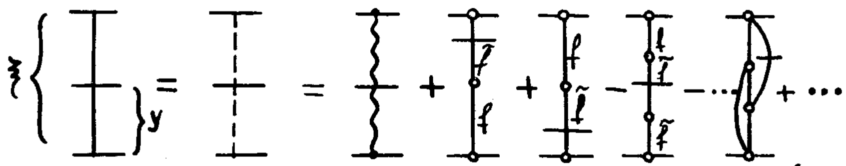

$$\tilde{f}(\xi,y) = \tilde{v}(\xi,y) = \tilde{\rho}_0(\xi,y) + \tilde{C}(\xi,y) + \tilde{\mathcal{D}}(\xi,y)$$

Fig. 17. The cut irreducible in s- channel graphs which give contribution to the one particle inclusive cross-section.

## References


1. V.N.Gribov, A.A.Migdal, Yad.Fiz. 10(1968) 1213.
2. A.J.Lendel, K.A.Ter-Martirosyan, JETP Lett. 11(1970)70.
3. K.G.Boreskov, A.M.Lapidus, S.T.Sukhorukov, K.A.Ter-Martirosyan, Yad.Fiz. 14 (1971) 814.
4. U.Amaldi, E.Biancastelli et al., Phys.Lett. 43B (1973) 321
5. S.Amedolia, G.Belletini et al., Phys.Lett. 44B (1973) 119.
6. V.N.Gribov, JETP 53 (1967) 654.
7. A.A.Migdal, A.M.Polyakov, K.A.Ter-Martirosyan, JETP 67(1974)84.
8. P.D.B.Collins, F.D.Gault, A.Martin, Phys.Lett. 47B(1973) 171; Nucl.Phys. B80 (1974) 135; Nucl.Phys. B83 (1974) 241.
9. A.Capella, J. Thanh Tran Wan, J.Kaplan. Preprint LPTHE 75/12,
10. H.Cheng, T.T.Wu, Phys.Rev.Lett. 24 (1970) 1456.
11. B.A.Abramovsky, V.N.Gribov, O.V.Kanchely, Yad.Fiz. 18(1973)595.
12. J.B.Bronzan, Preprint NAL-Pub-73/69-THY (1973).
13. J.L.Cardy, Nucl.Phys. B75(1974) 413.





14. M.S.Dubovikov, K.A.Ter-Martirosyan. Preprint ITEP-37,Moscow,1976.

B.Z.Kopeliovich, L.I.Lapidus, JETP 71 (1976),61;

JINR E2-9537, Dubna, 1976.

B.Z.Kopeliovich, Lecture at the XI Winter School of LNPI on Nuclear Physics and Elementary Particles, Leningrad,1976.

16. K.A.Ter-Martirosyan, JETP Letters 15(1972)734.
17. V.Barger, Proc. 17th Int. Conf. on High Energy Phys, London,1974.
18. B.Barger, J.Luthe, R.J.N.Phillips, Nucl.Phys. B88(1975) 237.
19. G.Auberson, T.Kinoshita, A.Martin, Phys.Rev. D3(1971)3185.
20. V.Barger, F.Halzen, T.K.Gaisser, C.J.J.Noble, G.B.Yodh, Phys.Rev.Lett. 33(1974) 1051.
21. O.V.Kanchely, JETP Lett. 18(1973) 469.
22. K.A.Ter-Martirosyan, Phys.Lett. 44B(1973) 377.
23. Z.Koba, M.B.Nielsen, P.Olesen, Nucl.Phys. B40(1972) 317.
24. H.D.I.Abarbanel, J.B.Bronzan, Phys.Rev. D9 (1974) 2397.
25. L.D.Soloviev, JETP Lett., 18(1973) 455.

L.D.Soloviev, A.V.Shelkachov, Particles and Nucleus, 6 (1975)571.

26. S.-J-Chang, T.-M-Yan, Phys.Rev.Lett. 25 (1970) 1586.

Phys.Rev. D4 (1971) 537.

27. B.M.Barbashov, V.V.Nesterenko, Yad.Fiz. 20(1974) 218.


Received by Publishing Department
on July 6, 1976.